YAP/TAZ-TEAD ACTIVITY LINKS MECHANICAL CUES TO SPECIFIC CELL FATE WITHIN THE HINDBRAIN BOUNDARIES

Adrià Voltes[1], Covadonga F Hevia[1], Chaitanya Dingare[2], Simone Calzolari[1+], Javier Terriente[1+], Caren Norden[3], Virginie Lecaudey[2], Cristina Pujades[1*]

[1]Department of Experimental and Health Sciences, Universitat Pompeu Fabra, 08003 Barcelona, Spain

[2]Goethe University, Frankfurt, Germany

[3]Max Planck Institute of Molecular Cell Biology and Genetics, Dresden, Germany

[+]Present address: ZeClinics, 08003 Barcelona, Spain

*Correspondence to:
Cristina Pujades, PhD
Department of Experimental and Health Sciences
Universitat Pompeu Fabra
PRBB, Dr Aiguader 88
08003 Barcelona, SPAIN
cristina.pujades@upf.edu
ORCID ID CP: 0000-0001-6423-7451

RUNNING TITLE: Yap/Taz-activity controls cell fate hindbrain boundaries

SUMMARY

How embryonic cells *in vivo* perceive their microenvironment through physical and mechanical cues during morphogenesis remains largely unexplored. Recently, the YAP/TAZ family of transcriptional co-activators has emerged as a fundamentally important regulator of cell proliferation and tissue regeneration, responding to cues from the extracellular matrix, cell shape and the actomyosin cytoskeleton. However, how signals are interpreted during embryonic tissue deformation resulting in specific cell fates has not been solved yet. In this work, we use the zebrafish hindbrain to explore how changes in tissue architecture during tissue segmentation affect gene expression and thereby ultimately inform cell decisions.

We unveil the role of Yap/Taz-TEAD activity in hindbrain boundaries as sensor and effector of mechanical signals in the regulation of cell fate upon hindbrain compartmentalization. We show that boundary cells respond to mechanical cues in a cell-autonomous manner through Yap/Taz-TEAD activity. Further, cell-lineage analysis reveals that Yap/Taz-TEAD active boundary cells display heterochronic proliferative capacity, and this switch in cell proliferation behavior results in changes of cell fate, from proliferating progenitors to differentiated neurons. Finally, functional experiments demonstrate the role of Yap/Taz-TEAD activity in maintaining the cell progenitor features in the hindbrain boundary cell population. Thus, our results suggest that changes in tissue architecture upon hindbrain segmentation work as informational systems affecting gene expression, and therefore cell fate during brain morphogenesis.

KEYWORDS: boundaries, compartments, mechanical cues, cell fate, progenitors, neurons

INTRODUCTION

Recently evidence emerged showing that mechanical signals are fundamental regulators of cell behavior. For example, extracellular matrix (ECM) rigidity, cell shape and the actomyosin cytoskeleton were found to direct cell behavior in vertebrates through the regulation of the downstream effectors of the Hippo pathway, such as YAP (Yes-associated protein) and TAZ (transcriptional co-activator with PDZ-binding motif) (Halder *et al*, 2012). A major layer of regulation of YAP and TAZ occurs at the level of their subcellular distribution, as the activation of YAP and TAZ entails their accumulation into the nucleus, where they bind to and activate TEAD transcription factors (Zhao *et al*, 2008). Here, YAP and TAZ, are able to interpret diverse biomechanical signals and transduce them into biological effects in a manner that is specific for the type of cell and the mechanical stress. For example, YAP localization can be regulated by mechanical cues such as ECM rigidity, strain, shear stress, adhesive area or force (Aragona *et al*, 2013; Benham-Pyle *et al*, 2015; Calvo *et al*, 2013; Chaudhuri *et al*, 2016; Dupont *et al*, 2011; Elosegui-Artola *et al*, 2016; 2017; Nakayama *et al*, 2017; Wada *et al*, 2011). Nevertheless, the role of YAP and TAZ and their regulation by the multitude of physical tissue deformations occurring during brain morphogenesis remains largely unexplored.

In this work, we address the role of tissue segmentation and mechanical cues in the regulation of cell diversity in the embryonic hindbrain. The hindbrain undergoes a dynamic self-organization with dramatic morphogenetic changes over time, whereby a sequence of mechanical and architectural checkpoints must occur to assess the final functional tissue outcome. This involves the segmentation of the tissue, which leads to the transitory formation of morphological buldges named rhombomeres (r1-r7). Each rhombomere constitute developmental units of gene expression and cell lineage compartments (Kiecker & Lumsden, 2005; Fraser *et al*, 1990; Jimenez-Guri *et al*, 2010). Compartmentalization involves the formation of a cellular interface between segments called hindbrain boundaries (Guthrie & Lumsden, 1991). Cells within these boundaries display specific features and serve distinct functions during embryonic development. First, when morphological rhombomeric segments arise boundary cells act as a

morphomechanical barrier to prevent cell intermingling. This is due to the enrichment of actomyosin cable-like structures at the apical side of boundary cells that generate tension allowing these cells to behave as an elastic mesh (Calzolari *et al*, 2014; Letelier *et al*, 2018). During neurogenesis, hindbrain boundaries constitute a node for signaling pathways instructing the differentiation and organization of neurons in the neighboring rhombomeres (Cheng *et al*, 2004; Riley *et al*, 2004; Cooke *et al*, 2005; Terriente *et al*, 2012). Moreover, boundary cells provide proliferating progenitors and differentiating neurons to the hindbrain (Peretz *et al*, 2016). However, how boundary cells make these functional transitions is largely unknown.

To answer this question, we characterized how morphogenetic changes during hindbrain segmentation are sensed and transduced into specific biological outcomes. We unveil that Yap/Taz-TEAD activity acts as a sensor of mechanical cues, and reveal by cell-lineage analysis a heterochrony in the proliferation of Yap/Taz-TEAD active boundary cells. This switch in cell proliferation behavior results in changes of cell fate -from progenitors to differentiated neurons-. Finally, using a combination of functional approaches we demonstrate that Yap/Taz-TEAD activity is essential for maintaining boundary cells as proliferative progenitors. Thus, changes in tissue architecture and mechanical forces instructed by the cellular microenvironment work as informational systems affecting gene expression, and therefore cell fate in hindbrain boundaries.

RESULTS

Hindbrain boundary cells display Yap/Taz-TEAD activity

During hindbrain segmentation, morphological boundaries are visible as shallow indentations on the outside of the neural tube (Maves *et al*, 2002; Calzolari *et al*, 2014). At this stage, the hindbrain boundary cells appear at the interface between rhombomeres (Figure 1A-D) and expand all along the dorsoventral domain of the hindbrain (Cheng *et al*, 2004). They express a specific set of genes (Letelier *et al*, 2018), and remarkably, no proneural genes. The latter are expressed in zones that flank rhombomere boundaries in which they drive neurogenesis (Nikolaou *et al*, 2009). In order to understand which cells contributed to the hindbrain boundaries, we characterized their rhombomeric origin by staining embryos with genes expressed at boundaries such as *rfng*, and in odd- and even-rhombomeric genes such as *egr2a* and *hoxb1a* (Figure 1A-D). We assessed that hindbrain boundaries are visible from 15hpf and constituted by a bilayer of cells contributed by adjacent rhombomeres; one cell layer expresses even-rhombomeric markers (Figure 1D-D'; see cells with white asterisk in D') whereas the other one does express odd-rhombomeric genes (Figure 1D-D'; see cells with black asterisk in D'). Boundary cells display different morphological features than their rhombomeric neighbors. They differ in shape -they are triangular-shaped (Gutzman & Sive, 2010)- and single cell segmentation showed that they displayed large apical footprints (Figure 1E-E'), compared with spindle-shaped rhombomeric cells that had smaller apical sides (Figure 1E,E''). Boundary cells do actively divide during early embryonic development as observed by BrdU incorporation (see white arrows in Figure 1F) and by life imaging of embryos (see non-magenta cell incurring into the magenta territory upon mitosis in Figure 1G-G', (Calzolari *et al*, 2014). Functionally, it was shown that these boundary cells act as an elastic mesh to prevent cell mixing between adjacent rhombomeres. This is due to the assembly of actomyosin cable-like structures in the apical side of these cells that generate tension within this cell population (Calzolari *et al*, 2014; Letelier *et al*, 2018). Given the compelling evidence for the relevance of YAP and TAZ as downstream mediators of mechanical cues, we investigated the role of Yap/Taz-TEAD activity within boundary cells as putative sensors of changes in cell and tissue architecture. Although *yap* is ubiquitously

expressed in the embryo (Agarwala *et al*, 2015), the Yap protein is enriched in hindbrain boundaries, and preferentially localized inside the nucleus when compared to rhombomeric cells (Figure 1H-H'', see arrows in H'' pointing to boundary cells where Yap and DAPI colocalized). To determine whether Yap was acting as a cofactor of transcription for TEAD protein in these cells, we monitored the TEAD activity *in vivo* by using the transgenic reporter line Tg[4xGTIIC:d2GFP] that carries a promoter containing 4 multimerized GTIIC sequences, which are consensus TEAD-binding sites (Miesfeld & Link, 2014). We evidenced that indeed boundary cells displayed Yap/Taz-TEAD activity at early stages of embryonic development (Figure 1I). Reporter transgene expression then served us as a direct read-out to visualize the effects of architectural constrains, since the signal was evident in the boundary cells either belonging to the odd- or even-rhombomeres (Figure 1J). Interestingly, not all boundary cells displayed Yap/Taz-TEAD activity (Figure 1K), and the TEAD-active cells also expressed Sox2, a marker for neural progenitors (Figure 1K'-K''). To dissect the contribution of Yap and Taz, we followed the TEAD-activity in Tg[4xGTIIC:d2GFP] embryos where either Yap or Taz was downregulated by splice- or translation-blocking morpholinos (Figure S1). As shown in Figure 1L-N, both YAP and TAZ contribute to TEAD-activity within the boundary cell population. Accordingly, when embryos were immunostained with anti-TAZ, staining was specifically allocated to hindbrain boundary cells (Figure 1O-O''). These results suggest that hindbrain boundaries harbor progenitors that display Yap/Taz-TEAD activity, and both YAP and TAZ are important to maintain this activity.

Establishment of Yap/Taz-TEAD activity in boundary cells

Next, we monitored the onset of Yap/Taz-activity by following GFP expression in embryos carrying the transgenic reporter Tg[4xGTIIC:d2GFP] (Miesfeld & Link, 2014). We found that the pathway is active from 20hpf, since transcription of the *gfp* mRNA can be visualized already at this stage (Figure 2A-C). However, GFP-positive boundary cells could be detected slightly later at 26hpf, and GFP was maintained in the boundaries until 72hpf (Figure 2D-F; data not shown). To distinguish early-born from late-born Yap/Taz-active boundary cells, we followed the BAPTI method (Birthdating Analysis by Photoconverted fluorescent Protein Tracing In vivo, Caron *et al*, 2008). We

used the KAEDE protein, which upon exposure to ultraviolet light (405 nm) is permanently cleaved making its emission spectrum shift from green to red (Ando *et al*, 2002). The converted KAEDE remains stable for several days (Hatta *et al*, 2006; Sapède *et al*, 2012). To specifically label Yap/Taz-active cells, we made use of the transgenic line carrying KAEDE under the control of the 4xGTIIC promoter (Tg[4xGTIIC:Gal4;UAS:KAEDE]) and photocoverted $KAEDE^G$ in the boundary cells in 30hpf embryos (Figure 2G). This resulted in red fluorescent-labeling of TEAD-active cells born before 30hpf (Figure 2H-H'''', see no $KAEDE^G$-cells in H'). At 48hpf, these early-born cells were still evident as presence of the converted red-fluorescent KAEDE was still observed ($KAEDE^R$ Figure 2I, I''-I'''). Because the KAEDE under the control of the Yap/Taz-activity reporter continued to be expressed in these cells, they also displayed *de novo* synthesized green-fluorescent KAEDE ($KAEDE^G$) (Figure 2I-I''). A close analysis to $KAEDE^G$-cells indicated that most of them expressed $KAEDE^R$ (compare Figure 2I' and I''), suggesting that Yap/Taz-TEAD activity in the hindbrain boundaries is triggered before 30hpf. In line with this, when KAEDE was photoconverted in embryos at 48hpf (Figure 2J-J'''), after complete photoconversion no $KAEDE^G$-cells were observed at 72hpf (Figure 2K') suggesting that the Yap/Taz-activity is shut off before 48hpf. At this stage, only $KAEDE^R$ labels the derivatives of Yap/Taz-active cells. Thus, our analysis confirmed that Yap/Taz-activity in the hindbrain boundary cells is switched on before 30hpf, just after boundary cells were important for preventing cell intermingling as a mechanical barrier (Calzolari *et al*, 2014). Overall, these results point to a putative role of YAP and TAZ as sensors of mechanical cues that control specific boundary cell properties.

Yap/Taz-TEAD activity senses mechanical cues in hindbrain boundary cells

Cues from the actomyosin cytoskeleton were found to converge on the regulation of YAP and TAZ in vertebrates (for reviews see Halder *et al*, 2012; Panciera *et al*, 2017). Our previous work demonstrated the role of contractile forces exerted by F-actin cables and their associated myosin motors to generate mechanical tension in boundary cells, specially through regulation of small GTPases of the RHO family (Calzolari *et al*, 2014; Letelier *et al*, 2018). Thus, our aim was to address whether integrity of the actomyosin cytoskeleton was necessary for Yap/Taz-activity within the

boundary cells. To do so, Yap/Taz-activity was determined after blunting endogenous tensile forces in the Tg[4xGTIIC:d2GFP] embryos by several means (Figure 3): i) inhibition of myosin II using pharmacological treatments such as *para*-Nitroblebbistatin or Rockout (Calzolari *et al*, 2014), ii) disruption of the actomyosin cable assembly by downregulating the function of the boundary specific small GTPase Rac3b, with splice-blocking morpholino (Letelier *et al*, 2018), and iii) conditional inhibition of Rac3b by clonal expression of a dominant negative form of Rac3b (Myc:hsp:Rac3bDN) (Letelier *et al*, 2018). Upon inhibition of myosin II before the onset of Yap/Taz-activity within the boundaries, the activity was lost (Figure 3B-C, Blebbistatin: n = 15/20 Rockout: n = 15/19; Figure 3F-H, Blebbistatin: n = 29/42; Rockout: n = 16/31) when compared with control embryos incubated with DMSO (Figure 3A, n = 3/20; and 3F, n = 8/36). This happened both using Blebbistatin, which inhibits myosin II by blocking the myosin heads in a complex with low actin affinity (Képiró *et al*, 2014), or using Rockout that blocks Rho kinase activity (Ernst *et al*, 2012). The same result was obtained by downregulating Rac3b with MO-Rac3b (Figure 3E, n = 31/38), whereas embryos injected with a random morpholino did not display this phenotype (Figure 3D, n = 4/22). In all cases, this downregulation was specifically significant in the boundary cell population, since Yap/Taz-activity within the somites was maintained (Figure 3B-C, E). This shows that tension was necessary for activating the Yap/Taz-pathway; however, it was not necessary for its maintenance since Yap/Taz-activity was not downregulated after inhibiting tensile forces from 26hpf onwards (Figure 3I-K; DMSO: n = 0/16; Blebbistatin: n = 6/24; Rockout: n = 5/19). The same result was obtained by conditional dowregulation of Rac3b (Figure 3M): Tg[4xGTIIC:d2GFP] embryos were injected either with hsp:Myc or Myc:hsp:Rac3bDN, heat-shocked and the percentage of clones within the boundaries that expressed green (Yap/Taz-activity) and red (Myc or Myc:Rac3bDN) were analyzed 16h later (Figure 3L). As displayed in Figure 3M, the majority of clones expressing Myc displayed Yap/Taz-activity (Figure 3N-N'', n = 20/21 see white cells in N''). On the contrary, the majority of boundary clones expressing Myc:Rac3bDN did not express Yap/Taz-activity (Figure 3O-O''', n = 33/47). Thus, YAP and TAZ respond to mechanical actin cues, most probably as mediators of these signals.

Yap/Taz-active boundary cells display heterochronic proliferative behavior

Next, we explored the lineage of Yap/Taz-active cells within the hindbrain in order to study their spatiotemporal dynamics. For this, we established a pipeline allowing us the cell lineage reconstruction and cell behavior analysis by 3D+time imaging (Movie S1, Figure 4A), and took advantage of the high temporal coverage and resolution provided by Single Plane Illumination Microscopy. We used several datasets encompassing the onset and offset of Yap/Taz-activity (Table 1, Figure S2). Tg[4xGTIIC:d2GFP] embryos were injected either at one-cell stage with hsp:H2B-RFP and heat-shocked at 26hpf or at 8 cell/stage with H2B-mCherry, and imaged as indicated in Movie S1 and Figure S2. The lineage of 63 single Yap/Taz-active cells (GFP-positive) expressing RFP/mCherry in the nucleus was reconstructed during approximately 20 hours of light sheet imaging (see Movie S1 as example). Cell behavior was assessed according to i) cell division (dividing/non-dividing; Figure 4A-D), and ii) cell differentiation (progenitor/differentiated; Figure 4E-I) status. Most of the cells that were tracked from 26hpf onwards actively proliferate (see: orange lines in Figure 4A, cell undergoing division and giving rise to four daughter cells in Figure B-B' and Movie S1). However, at 40hpf cells display a clear switch in their proliferative behavior and most of the tracked cells do not divide any further (see black lines in Figure 4A). Although at late stages cells do not express *di novo* GFP because no new activity is triggered (Figure 2), we can still track the derivatives of these cells thanks to the perdurance of the d2GFP protein. In line with this heterochronic behavior, when cells are photoconverted at 48hpf, the same number of red-derivatives than original photoconverted cells was obtained (Figure 4C-C'). Similar behavior was observed when cell proliferation is assessed by immunostaining with anti-PH3 antibody: the number of Yap/Taz-active boundary cells that undergo mitosis decreases upon embryonic development confirming this switch in the proliferative capacity (Figure 4D). In summary, the reconstruction of the lineage of Yap/Taz-active boundary cells from 4D *in vivo* data provides compelling and essential information about cellular/population dynamics and lineage relationships, demonstrating that Yap/Taz-active boundary cells display heterochronic proliferative behavior. This switch in proliferation coincides in time with the offset of Yap/Taz-activity.

In order to seek whether this change in proliferative capacity was related to the cell differentiation status (progenitor vs. differentiated neuron), we assessed the fate of

these very same tracked Yap/Taz-active cells over time by tracing their spatial distribution (position in the ventricular vs. mantle domains). First, to define where the border between the progenitor and the neuronal domain was, we generated a dynamic map of progenitors vs. differentiated neurons within the hindbrain boundary region. We analyzed how the neuronal differentiation territory changed during this time window by following the growth of the HuC-domain over time. We observed that the progenitor domain undergoes a dramatic reduction in size at the expense of the neuronal differentiation domain (Figure 4E). Quantification of the sizes of the progenitor/differentiation domains by measuring the Euclidian distances along the apical and basal edges of the neural tube showed that the growth of the HuC-domain cannot only be explained by overall growth of the tissue, but it required the decrease of the progenitor domain (Figure 4E-F). The use of Euclidean distances for measuring growth is equivalent to the use of the HuC-areas, as depicted in Figure 4G. Once the impact of morphogenesis in the distribution of the boundary cell populations was assessed, we plotted the position of the previously tracked Yap/Taz-active cells at different developmental stages on the top of this map, and use it as readout of their differentiation state. For this, we measured the distance of the nucleus of the tracked Yap/Taz-active cells to the ventricular zone at different time steps of the movie (Figure 4H). Nuclei located close to the apical side correspond to progenitor cells, whereas nuclei close to the basal side correspond to differentiated neurons. At the onset of Yap/Taz-activity, most of the tracked cells that undergo proliferation are found in the progenitor domain (see magenta dots on light grey histogram at 26hpf in Figure 4H), and upon time more Yap/Taz-active derivatives are found in the differentiation domain (see how more magenta dots are on dark grey histogram in Figure 4H). Although at 70hpf most of the Yap/Taz-active derivatives are located in the HuC-positive domain (dark grey histogram in Figure 4H), there is still a pool of TEAD-active derivatives remaining in the ventricular zone. This switch in nuclei position coincides with the previously observed heterochronic proliferative behavior, suggesting that Yap/Taz-active cells within the boundaries behave first as progenitors and once they switch off Yap/Taz-activity they become differentiated neurons. Most probably boundaries need to balance the ratio progenitors/differentiated neurons as other parts of the neural tube do (Hiscock *et al*, 2018). In accordance with this idea, and taking into

consideration the high perdurance of KAEDE, we observed Yap/Taz-derivatives in the neuronal differentiation domain that expressed HuC (see white arrows in Figure 4I-I'').

Yap/Taz-activity regulates cell fate in the hindbrain boundaries

To investigate whether Yap and Taz are conveying information about tissue mechanical properties into behavior of individual boundary cells, we performed functional studies and evaluated their effects in cell apoptosis and proliferative capacity. Since both YAP and TAZ contribute to TEAD-activity within the boundary cell population (Figure 1I-K), and considering that double homozygous mutants for *yap* and *wwtr* (*taz*) die at earlier stages than needed for the analyses, we undertook several alternative functional approaches (Figure 5). Loss-of-function of Yap/Taz-activity was assessed either by i) downregulating Yap with splice-blocking morpholinos (Figure S1A-D) in *wwtr* mutants (*wwtr*^{fu55}; Figure S1E, G), ii) using *yap/taz* compound mutants (*yap*^{fu48} *wwtr*^{fu55}; Figure S1E-G), and iii) by expressing dominant negative Yap or TEAD forms (DSRed:UAS:yapDN, DSRed:UAS:TEAD-DN; (Miesfeld *et al*, 2015) specifically in the Yap/Taz-active cells. Downregulation of Yap in the *wwtr*$^{fu55/+}$ mutant background had no effect on the number of apoptotic figures, neither in the boundaries (Figure 5A; Table 2) nor in the rhombomeric cells (Figure 5C; Table 3). On the other hand, when cell proliferation was assessed in *wwtr* mutants in which Yap was downregulated, they exhibited a decrease in the number of proliferating boundary cells (Figure 5B; Table 2), with no effect within the rhombomeric cells (Figure 5D, Table 3). We made use of *wwtr* heterozygous mutants (*wwtr*$^{+/fu55}$) injected with MO-Yap, because injection of MO-Yap in *wwtr* homozygous mutant embryos (*wwtr*^{fu55}) led to early mortality. This observation suggests that Yap/Taz-activity specifically regulates the proliferative capacity of hindbrain boundary cells. To underline this observation, we performed the same analysis by using a combination of *yap/wwtr* compound mutants (Figure 5E-H, Table 2-3). We obtained a similar set of results than in the previous experiment, namely Yap/Taz-activity did not regulate apoptosis within the hindbrain (Figure 5E,G; Table 2). However, when cell proliferation was analyzed the number of boundary cells undergoing mitosis was lower in *yap/wwtr* compound mutants with three mutated alleles (*yap*$^{fu48/+}$*wwtr*^{fu55} and *yap*^{fu48}*wwtr*$^{fu55/+}$) when compared to the rest of analyzed genotypes (Figure 5F; Table 2). Again, no defects were observed in any of the mutant

combinations when rhombomeric regions were analyzed (Figure 5H; Table 3). The penetrance of the phenotype is less profound in compound mutants, most probably due to genetic compensation as previously described (Rossi *et al*, 2015; Stainier *et al*, 2017). To study whether this is a cell-autonomous effect, we specifically decreased Yap/Taz-activity within the hindbrain boundary cells by injection of dominant negative forms of Yap (DsRed:UAS:Yap-DN) and TEAD (DsRed:UAS:TEAD-DN) in Tg[4xGTIIC:Gal4;UAS:KAEDE] embryos. Clones expressing DsRed-constructs were evaluated for cell size and position. In all cases in which TEAD-activity was downregulated, either by Yap- or TEAD-DN, we observed a decrease in the number of cells per clone (Figure 5I; DsRed:Yap-DN = 4,78 ± 0,34 cells/clone; DsRed:Tead-DN = 3,12 ± 0,29 cells/clone) when compared to control UAS:DsRed:injected embryos (6,54 ± 0,38 cells/clone). This demonstrated that indeed it is a cell-autonomous mechanism. Finally, to support the hypothesis that Yap/Taz-activity regulates cell proliferation and not transition towards the differentiation state, we followed the apico-basal position of cell clones upon inactivation of Yap/Taz. No changes in the clonal apico-basal distribution were obtained (Figure 5J; DsRed:Yap-DN = 94,52% of cells located in ventricular zone; DsRed:Tead-DN = 92,71% of cells located in ventricular zone; control DsRed = 92,43% of cells located in ventricular zone), suggesting that Yap/Taz-activity is not involved in transitioning cells to differentiation but mainly controlling the proliferative state of the progenitors. These results demonstrate that Yap and Taz are not only sensors, but also mediators of mechanical cues for the regulation of the size of the progenitor pool in the hindbrain boundaries.

DISCUSSION

How spatiotemporally controlled cell specification and differentiation occur alongside morphogenesis in the construction of the functional brain is an important area of study in developmental neuroscience. Here, we provide evidence that mechanical cues are sensed and transduced to regulate proliferative competence in the embryonic hindbrain boundaries. Mechanical inputs localize YAP/TAZ activity at sites of high mechanical stresses during tissue segmentation in the hindbrain boundaries. YAP/TAZ regulation serves as a transducer of physical properties of the microenvironment into a critical cell decision: to remain undifferentiated to keep the progenitor pool or to differentiate.

Upon hindbrain segmentation boundary cells are exposed to tension and act as an elastic mesh to prevent cell intermingling (Calzolari *et al*, 2014; Letelier *et al*, 2018), and most probably this would confine YAP/TAZ activity to the boundary cells exposed to mechanical stresses. After the segregation of lineages is accomplished, boundary cells are maintained in the progenitor state due to continued Yap/Taz-activity. This provides a progenitor pool for the hindbrain, whereas the neighboring territories undergo neurogenesis acting as proneural clusters. Overall, this could allow the maintenance of progenitor cells within the hindbrain, which could be used for development and maturation, or recruited for later events of central nervous system growth or repair. Since behavior of hindbrain boundary cells is influenced by mechanical signals, it is tempting to speculate that they might be directed towards specific cell fates tuning the strength and duration of Yap/Taz activity. Inactivation of Yap/Taz-signaling leads to the loss of progenitor properties such as proliferation. Thus, the demonstration that Yap/Taz-mechanotransduction can orient cell behavior in hindbrain boundaries highlights the importance of coordinating morphogenesis and cell fate. In line with this, it has been proposed that mechanoactivation of YAP/TAZ promotes epidermal stemness in somatic stem cells by regulating Notch (Totaro *et al*, 2017).

Once TEAD-activity is turned off, cell progenitors switch their proliferation behavior and undergo neuronal differentiation. This is supported by our cell lineage analysis, in which taking advantage of the perdurance of the reporter protein used to monitor

TEAD-activity we are able to trace the derivatives of the Yap/Taz-active cells once the pathway is off. Recently, it has been reported that mechanical forces are overarching regulators of YAP/TAZ in multicellular contexts for the control of organ growth (Aragona *et al*, 2013). Moreover, YAP and TAZ are typically found in the nucleus in somatic stem cells or progenitors, being proposed as determinants of stem cell state (Panciera *et al*, 2016). In line with this, our functional approaches indicate that indeed Yap/Taz-activity holds the boundary cells in the progenitor state by controlling their proliferative capacity, and suggests that levels of mechanical tension and cytosketal organization in rhombomeric territories are below the threshold required to activate the transcriptional effects of YAP and TAZ.

Remarkably, this is the first report in which TEAD-activity requires both effectors, YAP and TAZ. The reasons of the importance of this backup to maintain TEAD-activity are currently unclear. However, one plausible explanation is that they confer robustness to the system. In this line, we recently showed the importance of regulatory elements in ensuring specific gene expression at the hindbrain boundaries in order to attain cortical tension at the borders, particularly important when the cell segregation process is challenged (Letelier *et al*, 2018). The establishment and maintenance of compartment boundaries is of critical importance in tissue segmentation and body plan organization (Dahmann *et al*, 2011). Thus, our observations suggest that hindbrain boundaries are crucial developmental territories, and most likely YAP and TAZ are needed to confer robustness to the system.

Why do hindbrain boundary cells display different mechanical features, cell fate and functional properties than their neighbors? Boundary cells coordinately unfold distinct functional properties over the entire program of hindbrain morphogenesis, first as an elastic mesh to prevent cell intermingling (Calzolari *et al*, 2014), then as a node for signaling pathways (for review see Terriente & Pujades, 2015), and finally, they provide proliferating progenitors and differentiating neurons to the hindbrain (Figure 4; Peretz *et al*, 2016). It is appealing to speculate that hindbrain boundaries undergo a tinkering strategy (Jacob, 1977), and the biological structure is “co-opted” to provide different solutions to the current challenges. This would mean that boundaries would serve to distinct functions as development proceeds, providing different solutions to the system making it robust upon continuous challenges.

ACKNOWLEDGEMENTS

We thank Brian Link who kindly provided us constructs and reagents, and Jerome Solon for critically reading the manuscript. We would like to thank S Calatayud and M Linares for technical assistance, and Pujades lab for critical insights. This work was supported by La Marató-TV3 grant 345/C/2014 and Spanish Ministry of Economy and Competitiveness BFU2015-67400-P (MINECO-FEDER, UE) to CP, and Unidad de Excelencia María de Maetzu MDM-2014-0370 to DCEXS-UPF. AV is recipient of a predoctoral fellowship from LaCaixa, JT was a recipient of a postdoctoral Beatriu de Pinos fellowship (AGAUR, Generalitat de Catalunya). CP is recipient of an ICREA Academia award (Institució Catalana per la Recerca i Estudis Avançats, Generalitat de Catalunya).

AUTHOR CONTRIBUTIONS

AV and CP contributed to the concept, design, and analysis of the experiments. AV, CFH, CD, SC, and JT contributed to the execution of experiments. CN and VL were involved in the analysis of the results. CP wrote the manuscript.

CONFLICT OF INTERESTS

The authors do not have any conflict of interests.

STAR METHODS

Fish samples

Animals are treated according to the Spanish/European regulations for handling of animals in research. All protocols have been approved by the Institutional Animal Care and Use Ethic Committees and implemented according to European regulations. All experiments were carried out in accordance with the principles of the 3Rs.

Zebrafish (*Dario rerio*) embryos were obtained by mating of adult fish using standard methods. All zebrafish strains were maintained individually as inbred lines. For repairing rhombomeres 3 and 5, two transgenic lines were used: Mü4127, which is an enhancer trap line in which the trap KalTA4-UAS-mCherry cassette was inserted in the 1.5Kb downstream of *egr2a/krx20* gene (Distel *et al*, 2009); and Tg[elA:GFP] that is a stable reporter line where chicken element A from *egr2a* was cloned upstream of the *gfp* reporter (Labalette *et al*, 2011). Tg[4xGTIIC:d2GFP] line monitors Yap/Taz-TEAD activity (Miesfeld & Link, 2014). Tg[HuC:GFP] line labels early differentiated neurons (Park *et al*, 2000).

Transgenesis

Tg[4xGTIIC:Gal4; UAS:KAEDE] line was built up by injecting one-cell stage Tg[UAS:KAEDE] embryos with the 4xGTIIC:Gal4 vector generated using the Gateway technology (Life Technologies) and the Tol2 kit (Kwan *et al*, 2007). The 4xGTIIC promoter (Miesfeld & Link, 2014) was placed upstream of Gal4FF. One-cell stage embryos were co-injected with a 2nl volume containing 17.5ng/µl of Tol2 transposase mRNA and 15ng/µl of phenol:chloroform purified 4xGTIIC:Gal4 construct. Three or more stable transgenic lines derived from different founders were generated.

Cell segmentation

For manual segmentation of single cells, ITK-Snap software was used on embryos from Tg[CAAX:GFP]xMu4127 crosses (Figure 1). Single cells located either at the boundary or in the center of the rhombomere were segmented, and the resulting .vtk files were used to display them in FIJI-3D viewer.

Whole mount *in situ* hybridization

Zebrafish whole-mount *in situ* hybridization was adapted from (Thisse *et al*, 1993). The following riboprobes were generated by *in vitro* transcription from cloned cDNAs: *gfp*, *hoxb1a* and *egr2a* (Calzolari *et al*, 2014), and *rfng* (Cheng *et al*, 2004). *myl7* and *ephA4* were generated by PCR amplification (*myl7* Fw primer: 5'-GAC CAA CAG CAA AGC AGA CA-3', *myl7* Rv primer: 5'-TAA TAC GAC TCA CTA TAG GGT AGG GGG CAG CAG TTA CAG-3'; *epha4* Fw primer: 5'-AAG GAG CTA ACT CCA CCG TGC TC-3' and *epha4* Rv primer: 5'-TAA TAC GAC TCA CTA TAG GGA GAC ATC TGG GTC TTC CTC CAA A-3') from 24hpf embryos cDNA, adding T7 polymerase binding site at 5' of the reverse primers and followed by RNA transcription. The chromogenic *in situ* hybridizations were developed with NBT/BCIP (blue) and FastRed (red) substrates. For fluorescent *in situ* hybridization, DIG-labeled riboprobes were developed with fluorescein-tyramide substrate (TSA system). After staining, embryos were either flat-mounted and imaged under Leica DM6000B fluorescence microscope or whole-mounted in agarose and imaged under Leica MZ FLIII stereomicroscope or SP8 Leica confocal microscope.

In toto embryo immunostainings

For immunostaining, embryos were blocked in 5%Goat Serum in PBS-Tween20 (PBST) for 1h at room temperature and incubated O/N at 4°C with primary antibody. Primary antibodies were the following: anti-DsRed (1:500, Clontech), anti-GFP (1:200, Torrey Pines), anti-pH3 (1:200, Upstate), anti-Yap (1:100, Santa Cruz Biotechnology), anti-Taz (1:200, Cell Signaling, D24E4), anti-Sox2 (1:250, Abcam), and anti-Myc (1:200, Clontech). After extensive washings with PBST, embryos were incubated with secondary antibodies conjugated with Alexa Fluor®488 or Alexa Fluor®555 (1:500, Invitrogen). Draq5™ (1:2000, Biostatus, DR50200) or DAPI were used to label nuclei. Embryos were flat-mounted or whole-mounted in agarose, and imaged under a Leica SP5 or SP8 confocal microscope.

BrdU experiments and TUNEL assay

Embryos were incubated with 10μg/μl 5-Bromo-2´-desoxyuridine (Aldrich) for 2 hours prior to fixation. Afterwards they were incubated in 2N HCl for 30 minutes, three times washed in Sodium Borate pH 8.9 and processed for immunohistochemistry. Anti-BrdU BMC9318 antibody (Roche) was used in whole-mount at 1:200.

Distribution of apoptotic cells in the hindbrain was determined by TdT-mediated dUTP nick-end labeling (TUNEL) of the fragmented DNA. Briefly, after *ephA4 in situ* hybridization embryos were fixed for 30min with 4% (w/v) paraformaldehyde in PBS-Tween. Then, embryos were washed with PBS-Tween before being incubated with TUNEL reaction mixture for 1 hour at 37°C (Roche) followed by PBS-Tween washes. Fluorescein-labeled deoxynucleotides incorporated in apoptotic cells were visualized in a SP5 or SP8 Leica confocal microscopes.

Pharmacological treatments

Treatments with *para*-Nitroblebbistatin and Rockout were applied once the neural tube was already formed to avoid interfering with its early morphogenesis (Calzolari *et al*, 2014). Thus, in all experiments embryos at 14hpf were dechorionated and treated until 20hpf at 28.5°C with: i) myosin inhibitors such as *para*-Nitroblebbistatin (50nM) (Képiró *et al*, 2014) or Rockout (50nM), and ii) DMSO for control experiments. After treatment, embryos were fixed in 4%PFA for further analysis.

Antisense morpholinos and mRNA injections

For morpholino knockdowns, embryos were injected at one-cell stage with splicing-blocking morpholino oligomers (MOs) obtained from GeneTools, Inc. MOs were as follows: MO-p53 (Langheinrich et al., 2002), MO-Yap (Agarwala *et al*, 2015), MO-wwtr1 5'-CTG GAG AGG ATT ACC GCT CAT GGT C-3', MO-Rac3b (see MO-Rac3bSBI4E5 in (Letelier *et al*, 2018). For controls, random 25N morpholino was injected. MO-p53 was included in all MO-injections to diminish putative artifacts (Gerety & Wilkinson, 2011).
For mRNA expression, capped H2B-mcherry (Olivier et al, 2010), and lyn:GFP/mem:mCherry mRNAs were synthetized with mMessage mMachine (Ambion). Embryos were injected at one-cell stage and developed until the desired stages.

Photoconversion experiments

Tg[4xGTIIC:Gal4; UAS:KAEDE] embryos at 30hpf or 48hpf were anesthetized and mounted dorsally in 1%LMP-agarose. KAEDE^{G} was fully photoconverted with UV light (λ=405 nm) using a 20x objective in a Leica SP8 system. Upon exposure of UV light KAEDE protein irreversibly shifts emission from green to red fluorescence (516 to 581).

To make sure that all cells within the hindbrain were hit, we did an accurate analysis using confocal microscopy and YZ confocal cross-sections. In the case of the photoconversion of single-KAEDE^{G} cells, embryos at 30hpf expressing mosaic 4xGTIIC:Gal4;UAS:KAEDE were used. In all cases, after photoconversion embryos were returned to embryo medium with phenylthiourea (PTU) in a 28.5°C incubator. At 48hpf or 72hpf, embryos were mounted dorsally and imaged in vivo on a Leica SP8 system using PMT detectors and a 20x objective.

Conditional overexpression

Myc:hsp:Rac3bDN (T71N-mutation) construct was generated by site-directed mutagenesis (QuikChange Site-Directed Mutagenesis Kit, Stratagene #200518), and cloned into the MCS of a Tol2-based custom vector containing a heat shock promoter (hsp) and a Myc-tag (Letelier *et al*, 2018). Tg[4xGTIIC:d2GFP] embryos were injected at one-cell stage, grown at 28.5°C, and heat-shocked at 14hpf. All embryos were fixed at 18-20hpf, co-immunostained for Myc and GFP, and imaged for further analysis.

UAS:DsRed, DsRed:UAS:YapDN or DsRed:UAS:TeadDN constructs were injected in Tg[4xGTIIC:Gal4;UAS:KAEDE] embryos at one-cell stage. Embryos were grown until 24hpf, fixed, Draq5-stained and imaged under the confocal. Size of the clones was analyzed by quantifying nuclei in DsRed-positive boundary clones

3D+time imaging

Time-lapse movie for in vivo analysis of cell divisions in the rhombomeric boundaries

Anesthetized live double transgenic Tg[CAAX:GFP]xMu4127 embryos were embedded in 1% low-melting point (LMP) agarose with the hindbrain positioned towards the glass-bottom of the Petri dish in order to have a dorsal view with an inverted objective. The video was obtained with an inverted SP5 Leica confocal microscope and processed and analyzed using Fiji software (NIH). Experimental parameters for the video were: voxel dimension (nm): x 267.8 y 267.8 z 629.4, time frame: 10min; total time: 8h; pinhole: 1 Airy; zoom: 2.8; objective: 20x immersion; NA: 0.70.

Single-cell tracking experiments

Embryos were anesthetized using 0,04% MS-222 (Sigma) and mounted in 0,6% LMP-agarose in glass capillaries. Time-lapse imaging was performed at 28.5°C on a Zeiss

Lightsheet Z.1 microscope. Tg[4xGTIIC:d2GFP] embryos were injected with hsp::H2B-RFP or H2B-mCherry DNA at 1-8cell stage. Embryos injected with hsp::H2B-RFP were heat-shocked for 20min 2h before imaging. The cohort of embryos and datasets used in this study are depicted in Table 1 and Figure EV2. Each dataset corresponds to the imaging of a distinct embryo hindbrain. The videos were analyzed and cells manually tracked using Fiji software (NIH). Experimental parameters were: voxel dimension (nm): x 235.5 y 235.5 z 1000, time frame: see Table 1; total time: see Table 1; zoom: 1; objective: 20x water-dipping; NA: 1.

TALEN-genome editing

The mutant lines *yap*^{fu48} and *wwtr1*^{fu55} were generated using TALEN-induced mutagenesis strategy. A target site in the first exon and the corresponding left and right TALENs were designed using the online software MojoHand (http://www.talendesign.org). The TALENs were cloned using the TALEN repeat array plasmid library (Addgene kit #1000000024) and Golden Gate Assembly (Cermak *et al*, 2011). The detailed protocol is available on the Addgene website (https://www.addgene.org/static/cms/filer_public/98/5a/985a6117- 7490-4001-8f6a-24b2cf7b005b/golden_gate_talen_assembly_v7.pdf). The plasmids containing the RVDs fused to Fok1 were linearized with BamHI and corresponding RNAs were *in vitro* transcribed using the T3 mMessage mMachine Kit (Ambion by Life Technologies GmbH, Darmstadt, Germany). The left and right TALEN mRNAs were co-injected in one-cell stage embryos and several mutant alleles were recovered by amplifying a region encompassing the target site by PCR and digesting it with KpnI and PagI which are present in the spacer in the *yap1* and *wwtr1* wild type sequences, respectively (Figure EV1E). Zygotic mutants obtained from an incross of heterozygous mutant fish were raised to adulthood to obtain F3 maternal-zygotic (MZ) mutants. Zygotic wild type “cousins” obtained from the incross of the heterozygous mutant fish were raised and used as littermate controls for the MZ mutant fish.

Mapping the progenitor and neuronal domains within the hindbrain boundaries

Live Tg[HuC:GFP]xMu4127 embryos were imaged at 26, 40 and 70 hpf under a Leica SP8 confocal. Mu4127 staining was used as a landmark for rhombomeric interfaces. Fiji

was used in order to measure the length expanding from the apical ventricular zone edge (AVZE) of the neural tube to the basal mantle zone edge in r3/r4 and r4/r5, and this was called AVZE-BMZE length (orange line, Figure 4E). The boundary neuronal domain corresponds to the length encompassing the GFP-expressing territory (dark grey, Figure 4F). On the other hand, the boundary progenitor domain corresponds to the subtraction of the neuronal length to the total distance (light grey, Figure 4F). The temporal dynamics of the ratio (neuronal AVZE-BMZE length) / (total AVZE-BMZE length) was plotted and compared to the ratio (neuronal area) / (whole hemisphere area) (Figure 4G).

The position of the tracked nuclei relative to the total AVZE-BMZE length was plotted (Figure 4H). Aiming at displaying the data with anatomical coherence, the ratio (position of the nucleus) / AVZE-BMZE length was subtracted to 1, so values closer to 1 correspond to the cell position in the ventricular zone, thus the progenitor domain (Figure 4H).

Phenotypic analyses

Morphant mutants and compound mutants

Embryos were fixed with PFA 4% at 36 hpf. Fluorescent *in situ* hybridization for *epha4* was carried out in order to have the boundary landmarks for r3 and r5. Since hindbrain boundaries are located at the interface between adjacent rhombomeres (Figure 1D-D'), the last row of cells *epha4*-negative and the first row of *epha4*-positive cells (or the other way around depending on the interface) constitute the boundary cell population. Hence, *in situ* hybridization for *epha4* allows the localization of r2/r3, r3/r4, r4/r5 and r5/r6 boundaries. Embryos were imaged under the Leica SP8 confocal. Apoptotic (TUNEL) and proliferating (PH3-expressing) boundary cells were quantified at r3/r4 and r4/r5, whereas r5 was the rhombomeric territory used for non-boundary cell population analysis.

Clonal analysis

Injected embryos were fixed with PFA 4% at 36hpf and stained for Draq5. The size of the clones in the boundaries was assessed by quantifying the number of DsRed-nuclei. On the other hand, cell fate was analyzed according to cell position in the neural tube,

being progenitor cells those in contact to the ventricle. The percentage of ventricular cells per clone was plotted.

REFERENCES

Agarwala S, Duquesne S, Liu K, Boehm A, Grimm L, Link S, König S, Eimer S, Ronneberger O & Lecaudey V (2015) Amotl2a interacts with the Hippo effector Yap1 and the Wnt/β-catenin effector Lef1 to control tissue size in zebrafish. *Elife* **4:** e08201

Ando R, Hama H, Yamamoto-Hino M, Mizuno H & Miyawaki A (2002) An optical marker based on the UV-induced green-to-red photoconversion of a fluorescent protein. *Proceedings of the National Academy of Sciences* **99:** 12651–12656

Aragona M, Panciera T, Manfrin A, Giulitti S, Michielin F, Elvassore N, Dupont S & Piccolo S (2013) A mechanical checkpoint controls multicellular growth through YAP/TAZ regulation by actin-processing factors. *Cell* **154:** 1047–1059

Benham-Pyle BW, Pruitt BL & Nelson WJ (2015) Cell adhesion. Mechanical strain induces E-cadherin-dependent Yap1 and β-catenin activation to drive cell cycle entry. *Science* **348:** 1024–1027

Calvo F, Ege N, Grande-Garcia A, Hooper S, Jenkins RP, Chaudhry SI, Harrington K, Williamson P, Moeendarbary E, Charras G & Sahai E (2013) Mechanotransduction and YAP-dependent matrix remodelling is required for the generation and maintenance of cancer-associated fibroblasts. *Nature Cell Biology* **15:** 637–646

Calzolari S, Terriente J & Pujades C (2014) Cell segregation in the vertebrate hindbrain relies on actomyosin cables located at the interhombomeric boundaries. *EMBO J.* **33:** 686–701

Caron SJC, Prober D, Choy M & Schier AF (2008) In vivo birthdating by BAPTISM reveals that trigeminal sensory neuron diversity depends on early neurogenesis. *Development* **135:** 3259–3269

Cermak T, Doyle EL, Christian M, Wang L, Zhang Y, Schmidt C, Baller JA, Somia NV, Bogdanove AJ & Voytas DF (2011) Efficient design and assembly of custom TALEN and other TAL effector-based constructs for DNA targeting. *Nucleic Acids Research* **39:** e82–e82

Chaudhuri O, Gu L, Klumpers D, Darnell M, Bencherif SA, Weaver JC, Huebsch N, Lee H-P, Lippens E, Duda GN & Mooney DJ (2016) Hydrogels with tunable stress relaxation regulate stem cell fate and activity. *Nat Mater* **15:** 326–334

Cheng Y-C, Amoyel M, Qiu X, Jiang Y-J, Xu Q & Wilkinson DG (2004) Notch activation regulates the segregation and differentiation of rhombomere boundary cells in the zebrafish hindbrain. *Developmental Cell* **6:** 539–550

Cooke JE, Kemp HA & Moens CB (2005) EphA4 is required for cell adhesion and rhombomere-boundary formation in the zebrafish. *Current Biology* **15:** 536–542

Dahmann C, Oates AC & Brand M (2011) Boundary formation and maintenance in tissue development. *Nature Publishing Group* **12:** 43–55

Distel M, Wullimann MF & Köster RW (2009) Optimized Gal4 genetics for permanent gene expression mapping in zebrafish. *Proc. Natl. Acad. Sci. U.S.A.* **106:** 13365–13370

Dupont S, Morsut L, Aragona M, Enzo E, Giulitti S, Cordenonsi M, Zanconato F, Le Digabel J, Forcato M, Bicciato S, Elvassore N & Piccolo S (2011) Role of YAP/TAZ in mechanotransduction. *Nature* **474:** 179–183

Elosegui-Artola A, Andreu I, Beedle AEM, Lezamiz A, Uroz M, Kosmalska AJ, Oria R, Kechagia JZ, Rico-Lastres P, Le Roux A-L, Shanahan CM, Trepat X, Navajas D, Garcia-Manyes S & Roca-Cusachs P (2017) Force Triggers YAP Nuclear Entry by

Regulating Transport across Nuclear Pores. *Cell* **171:** 1397–1410.e14

Elosegui-Artola A, Oria R, Chen Y, Kosmalska A, Pérez-González C, Castro N, Zhu C, Trepat X & Roca-Cusachs P (2016) Mechanical regulation of a molecular clutch defines force transmission and transduction in response to matrix rigidity. *Nature Cell Biology* **18:** 540–548

Ernst S, Liu K, Agarwala S, Moratscheck N, Avci ME, Dalle Nogare D, Chitnis AB, Ronneberger O & Lecaudey V (2012) Shroom3 is required downstream of FGF signalling to mediate proneuromast assembly in zebrafish. *Development* **139:** 4571–4581

Fraser S, Keynes R & Lumsden A (1990) Segmentation in the chick embryo hindbrain is defined by cell lineage restrictions. *Nature* **344:** 431–435

Gerety SS & Wilkinson DG (2011) Morpholino artifacts provide pitfalls and reveal a novel role for pro-apoptotic genes in hindbrain boundary development. *Developmental Biology* **350:** 279–289

Guthrie S & Lumsden A (1991) Formation and regeneration of rhombomere boundaries in the developing chick hindbrain. *Development* **112:** 221–229

Gutzman JH & Sive H (2010) Epithelial relaxation mediated by the myosin phosphatase regulator Mypt1 is required for brain ventricle lumen expansion and hindbrain morphogenesis. *Development* **137:** 795–804

Halder G, Dupont S & Piccolo S (2012) Transduction of mechanical and cytoskeletal cues by YAP and TAZ. *Nat Rev Mol Cell Biol* **13:** 591–600

Hatta K, Tsujii H & Omura T (2006) Cell tracking using a photoconvertible fluorescent protein. *Nature Protocols* **1:** 960–967

Hiscock TW, Miesfeld JB, Mosaliganti KR, Link BA & Megason SG (2018) Feedback between tissue packing and neurogenesis in the zebrafish neural tube. *Development* **145:**

Jacob F (1977) Evolution and tinkering. *Science* **196:** 1161–1166

Jimenez-Guri E, Udina F, Colas J-F, Sharpe J, Padrón-Barthe L, Torres M & Pujades C (2010) Clonal analysis in mice underlines the importance of rhombomeric boundaries in cell movement restriction during hindbrain segmentation. *PLoS ONE* **5:** e10112

Képiró M, Várkuti BH, Végner L, Vörös G, Hegyi G, Varga M & Málnási-Csizmadia A (2014) para-Nitroblebbistatin, the non-cytotoxic and photostable myosin II inhibitor. *Angew. Chem. Int. Ed. Engl.* **53:** 8211–8215

Kiecker C & Lumsden A (2005) Compartments and their boundaries in vertebrate brain development. *Nature Reviews Neuroscience* **6:** 553–564

Kwan KM, Fujimoto E, Grabher C, Mangum BD, Hardy ME, Campbell DS, Parant JM, Yost HJ, Kanki JP & Chien C-B (2007) The Tol2kit: a multisite gateway-based construction kit for Tol2 transposon transgenesis constructs. *Dev. Dyn.* **236:** 3088–3099

Labalette C, Bouchoucha YX, Wassef MA, Gongal PA, Le Men J, Becker T, Gilardi-Hebenstreit P & Charnay P (2011) Hindbrain patterning requires fine-tuning of early krox20 transcription by Sprouty 4. *Development* **138:** 317–326

Letelier J, Terriente J, Belzunce I, Voltes A, Undurraga CA, Polvillo R, Devos L, Tena JJ, Maeso I, Rétaux S, Gómez-Skarmeta JL, Martínez-Morales JR & Pujades C (2018) Evolutionary emergence of the rac3b/rfng/sgca regulatory cluster refined mechanisms for hindbrain boundaries formation. *Proc. Natl. Acad. Sci. U.S.A.* **115:**

E3731–E3740

Maves L, Jackman W & Kimmel CB (2002) FGF3 and FGF8 mediate a rhombomere 4 signaling activity in the zebrafish hindbrain. *Development* **129:** 3825–3837

Miesfeld JB & Link BA (2014) Establishment of transgenic lines to monitor and manipulate Yap/Taz-Tead activity in zebrafish reveals both evolutionarily conserved and divergent functions of the Hippo pathway. *MECHANISMS OF DEVELOPMENT* **133:** 177–188

Miesfeld JB, Gestri G, Clark BS, Flinn MA, Poole RJ, Bader JR, Besharse JC, Wilson SW & Link BA (2015) Yap and Taz regulate retinal pigment epithelial cell fate. *Development* **142:** 3021–3032

Nakayama Y, Inomata C, Yuikawa T, Tsuda S & Yamasu K (2017) Comprehensive analysis of target genes in zebrafish embryos reveals gbx2 involvement in neurogenesis. *Developmental Biology*

Nikolaou N, Watanabe-Asaka T, Gerety S, Distel M, Köster RW & Wilkinson DG (2009) Lunatic fringe promotes the lateral inhibition of neurogenesis. *Development* **136:** 2523–2533

Panciera T, Azzolin L, Cordenonsi M & Piccolo S (2017) Mechanobiology of YAP and TAZ in physiology and disease. *Nat Rev Mol Cell Biol* **18:** 758–770

Panciera T, Azzolin L, Fujimura A, Di Biagio D, Frasson C, Bresolin S, Soligo S, Basso G, Bicciato S, Rosato A, Cordenonsi M & Piccolo S (2016) Induction of Expandable Tissue-Specific Stem/Progenitor Cells through Transient Expression of YAP/TAZ. *Cell Stem Cell* **19:** 725–737

Park HC, Kim CH, Bae YK, Yeo SY, Kim SH, Hong SK, Shin J, Yoo KW, Hibi M, Hirano T, Miki N, Chitnis AB & Huh TL (2000) Analysis of upstream elements in the HuC promoter leads to the establishment of transgenic zebrafish with fluorescent neurons. *Developmental Biology* **227:** 279–293

Peretz Y, Eren N, Kohl A, Hen G, Yaniv K, Weisinger K, Cinnamon Y & Sela-Donenfeld D (2016) A new role of hindbrain boundaries as pools of neural stem/progenitor cells regulated by Sox2. *BMC Biol.* **14:** 57

Riley BB, Chiang M-Y, Storch EM, Heck R, Buckles GR & Lekven AC (2004) Rhombomere boundaries are Wnt signaling centers that regulate metameric patterning in the zebrafish hindbrain. *Dev. Dyn.* **231:** 278–291

Rohrschneider MR, Elsen GE & Prince VE (2007) Zebrafish Hoxb1a regulates multiple downstream genes including prickle1b. *Developmental Biology* **309:** 358–372

Rossi A, Kontarakis Z, Gerri C, Nolte H, Hölper S, Krüger M & Stainier DYR (2015) Genetic compensation induced by deleterious mutations but not gene knockdowns. *Nature* **524:** 230–233

Sapède D, Dyballa S & Pujades C (2012) Cell lineage analysis reveals three different progenitor pools for neurosensory elements in the otic vesicle. *J. Neurosci.* **32:** 16424–16434

Stainier DYR, Raz E, Lawson ND, Ekker SC, Burdine RD, Eisen JS, Ingham PW, Schulte-Merker S, Yelon D, Weinstein BM, Mullins MC, Wilson SW, Ramakrishnan L, Amacher SL, Neuhauss SCF, Meng A, Mochizuki N, Panula P & Moens CB (2017) Guidelines for morpholino use in zebrafish. *PLoS Genet* **13:** e1007000

Terriente J & Pujades C (2015) Cell segregation in the vertebrate hindbrain: a matter of boundaries. *Cell. Mol. Life Sci.* **72:** 3721–3730

Terriente J, Gerety SS, Watanabe-Asaka T, Gonzalez-Quevedo R & Wilkinson DG (2012)

Signalling from hindbrain boundaries regulates neuronal clustering that patterns neurogenesis. *Development* **139:** 2978–2987

Thisse C, Thisse B, Schilling TF & Postlethwait JH (1993) Structure of the zebrafish snail1 gene and its expression in wild-type, spadetail and no tail mutant embryos. *Development* **119:** 1203–1215

Totaro A, Castellan M, Battilana G, Zanconato F, Azzolin L, Giulitti S, Cordenonsi M & Piccolo S (2017) YAP/TAZ link cell mechanics to Notch signalling to control epidermal stem cell fate. *Nature Communications* **8:** 15206

Wada K-I, Itoga K, Okano T, Yonemura S & Sasaki H (2011) Hippo pathway regulation by cell morphology and stress fibers. *Development* **138:** 3907–3914

Zhao B, Ye X, Yu J, Li L, Li W, Li S, Yu J, Lin JD, Wang C-Y, Chinnaiyan AM, Lai Z-C & Guan K-L (2008) TEAD mediates YAP-dependent gene induction and growth control. *Genes & Development* **22:** 1962–1971

FIGURE LEGENDS

Figure 1: Hindbrain boundary cells display Yap/Taz-activity.

A-D) Whole mount double *in situ* hybridization with *egr2a* (A-B,D), which labels rhombomeres (r) 5 and 6, or *hoxb1a* (C) labeling r4, and *rfng* labeling hindbrain boundaries in embryos at indicated developmental stages. D') Insert of the r4/r5 boundary. Note that *rfng* staining expands two cell layers: one expressing *egr2a/rfng* (see cells with black asterisk in D') and the other only *rfng* (see cells with white asterisk in D'). E) Double transgenic Tg[ubi:CAAX-GFP]Mu4127 embryo displaying GFP in the plasma membrane (shown in white) and mCherry in r3 and r5 (shown in magenta). Inserts in (E') and (E'') display dorsal (left) and lateral (right) views of manually segmented single cells from r3/r4 boundary (E') and r4 (E''), with the apical side at the bottom of the image. Note that the r3/r4 cell has a triangular shape with a large apical side, whereas r4 cell is spindle-shaped. F) BrdU-staining of a Mu4127 embryo at 18hpf. Note that cells at the boundaries display BrdU staining in green. G) 24hpf time-lapse stack (T_1) of a Tg[ubi:CAAX-GFP]Mu4127 embryo. G') Inserts from T_1-T_3 of the region framed in (G). Note that a cell upon division challenges the boundary. H) Whole mount anti-Yap immunostaing of a 26hpf embryo. H'-H'') Close ups from a non-boundary territory (H') and a boundary (H''): note that Yap is preferentially located into the nucleus in boundary cells (see white arrow in H''). I) Maximal Intensity Projection (MIP) of the hindbrain of a Tg[4xGTIIC:d2GFP] embryo at 36hpf displaying cells with Yap/Taz-activity in green. J) Tg[4xGTIIC:d2GFP]Mu4127 embryo displaying GFP in the boundary cells. Note that green cells displaying Yap/Taz activity are located in the boundaries between rhombomeres. K-K'') Immunostaining with anti-Sox2 (magenta) of Tg[4xGTIIC:d2GFP] embryo at 36hpf. Note in the reconstructed transverse section at the level of r4/r5 displayed with separated and merged channels that all green cells express Sox2. L-N) Analysis of Yap/Taz-activity in embryos where Yap or Taz were downregulated using splice blocking morpholinos (MO-control: n = 16; MO-Yap: n = 23). O-O'') Whole mount anti-Taz immunostaing of a 26hpf embryo showing that Taz is mainly localized in boundary cells. O'-O'') Inserts from (O), either at the level of the rhombomere (O') or the boundaries (O''). All images are dorsal views with anterior to the left, except for (K-K''), which is a reconstructed transverse section.

Figure 2: Birthdating of Yap/Taz-TEAD activity in the hindbrain boundaries.

A-C) Tg[4xGTIIC:d2GFP] embryos assayed for a whole mount *in situ* hybridization with a *gfp* mRNA probe at the indicated stages. Note that expression of *gfp* –and therefore Yap/Taz-activity- is already visible in the boundaries at 20hpf. Lateral views with anterior to the left. D-F) Expression of GFP in the hindbrain boundaries in Tg[4xGTIIC:d2GFP] embryos at 26hpf, 36hpf and 46hpf. Note that GFP is first observed at 26hpf and present until 72hpf (data not shown). Dorsal views with anterior to the left. G) Scheme depicting the BAPTI experiment: $Kaede^G$ in the hindbrain boundaries of Tg[4xGTIIC:Gal4FF;UAS:KAEDE] embryos was photoconverted to $Kaede^R$ at T_0, and embryos were let to develop until the desired stage (T_1). H-I) Embryo in which $Kaede^G$ was photoconverted to $Kaede^R$ at $T_{0=}$30hpf (H-H’’’) and analyzed at $T_{1=}$48hpf (I-I’’’). Note that new $Kaede^G$ appears at 48hpf (see merged channels in I’’-I’’’). J-K) Embryo in which $Kaede^G$ was photoconverted to $Kaede^R$ at $T_{0=}$48hpf (J-J’’’) and analyzed at $T_{1=}$72hpf (K-K’’’). Note that no $Kaede^G$ is observed after photoconversion (K-K’’’). Reconstructed transverse sections except for (H’’’,I’’’,J’’’,K’’’) that are dorsal views with anterior to the left.

Figure 3: Yap/Taz in the hindbrain boundaries sense mechanical cues.

A-E) Whole mount *gfp* in situ hybridization of Tg[4xGTIIC:d2GFP] embryos treated with DMSO (A), and myosin II inhibitors such as Blebbistatin (B) and Rockout (C), or injected with MO-control (D) or MO-Rac3b in order to downregulate Rac3b (E). Note that in all experimental cases *gfp* expression is downregulated in the hindbrain boundaries and not affected in the somites. Lateral views with anterior to the left. F-K) Expression of GFP in Tg[4xGTIIC:d2GFP] embryos treated with DMSO (F,I), and myosin II inhibitors such as Blebbistatin (G,J) and Rockout (H,K) at different intervals. Dorsal views with anterior to the left. L) Scheme depicting the experiment: Tg[4xGTIIC:d2GFP] embryos were injected with hsp:Myc or Myc:hsp:Rac3DN, heat-shocked at 14hpf and the phenotype was scored at 30hpf. M) Histogram displaying the % of cells expressing GFP (dark grey) of the Myc-positive cells (light grey) in control (hsp:Myc, N-N’’) and experimental conditions where the mechanical cues were compromised (Myc:hsp:Rac3DN, O-O’’).

Figure 4: Yap/Taz-active boundary cells display heterochronic proliferative behavior

A) Representation of the Yap/Taz-active cell lineage tree with branches indicating cell divisions. The 63 cell lineages are displayed from the moment of tracking onwards and color-coded according to proliferative behavior (orange: dividing; black: non-dividing). Each line corresponds to a single cell starting from the beginning of the track until the end of it (Table 1, Figure EV2). The Y-axis displays the time of embryonic development in hours post-fertilization (hpf). Note the cell behavioral switch from 40hpf, where most of the Yap/Taz-active cells do not divide anymore. B-B') Stills of a time-lapse movie from a single cell followed from 26hpf till 48hpf: the cell undergoes two cell divisions giving rise to 4 cells (see Movie EV1). C-C') Example of a group of three cells photoconverted at 48hpf and followed until 72hpf. Note that the number of cells does not change during these 24h. D) Graph showing the decrease in the number of Yap/Taz-TEAD proliferating boundary cells upon time. At 26hpf, approximately 20% of Yap/Taz-TEAD boundary cells are in mitosis, and this decreases dramatically at 40hpf. E) Scheme depicting the dramatic change in the progenitor (light grey) and neuronal (dark grey) domains of the hindbrain boundaries from 26hpf to 70hpf. Drawings are based in the analysis of the Tg[HuC:GFP] embryos at the given stages. F) Histogram displaying the actual size of the progenitor/neuronal domains at 26hpf, 40hpf, and 70hpf. Results were obtained from Tg[HuC:GFP] embryos where the AVZE-BMZE length (the length expanding from the apical ventricular zone edge –AVZE- of the neural tube to the basal mantle zone -BMZE- according to how cells are oriented within the neural epithelium) of 8-10 boundaries (4-5 embryos) per stage were measured. G) Comparison of the ratio obtained from measurements of HuC distances between the ventricular and mantle borders, with the measurement of the HuC area of an average of 12-18 boundaries (6-9 embryos) to show that both approaches are equivalent for the estimate of the progenitor/neuronal domain progression. H) Cells tracked in (A) were analyzed at different times and the distance of their nucleus to the apical side was measured according to the scheme. This value was used to calculate the position of the cell nucleus within the neural tube, considering the size of the thickness of the neural tube. Values were plotted (magenta dots) and overlaid with the information obtained from the progenitor/neuronal domain (see Star Methods). Note that most of the cell nuclei at 26hpf lay within the progenitor domain, whereas at

70hpf they do so in the neuronal differentiated domain. I-I'') Immunostaining of Tg[4xGTIIC:Gal4FF;UAS:KAEDE] embryos with anti-HuC at 50hpf, showing derivatives of Yap/Taz-active cells within the HuC-domain.

Figure 5: Yap/Taz-activity regulates cell proliferation in the hindbrain boundaries.
A-D) Wild type (*wwtr*$^{+/+}$), heterozygous (*wwtr*$^{fu55/+}$), or homozygous (*wwtr*^{fu55}) embryos for *taz* mutations were injected with MO-control or MO-Yap and the number of apoptotic (A,C) and proliferating (B,D) cells within the hindbrain boundaries (A-B; Table 2) or r5 (C-D; Table 3) were quantified. Each dot corresponds to the number of scored cells in a single boundary/rhombomere. P values for (B) are the following: MO-Control *wwtr*$^{+/+}$ vs. MO-Yap *wwtr*$^{fu55/+}$, p = 0.0008; MO-Control *wwtr*$^{fu55/+}$ vs. MO-Yap *wwtr*$^{fu55/+}$, p = 0.0026; MO-Control *wwtr*^{fu55} vs. MO-Yap *wwtr*$^{fu55/+}$, p = 0.0361; MO-Yap *wwtr*$^{+/+}$ vs. MO-Yap *wwtr*$^{fu55/+}$, p = 0.0027. E-F) Wild type (*yap*$^{+/+}$*wwtr*$^{+/+}$), double heterozygous (*yap*$^{fu48/+}$*wwtr*$^{fu55/+}$), or compound mutant (*yap*$^{fu48/+}$*wwtr*^{fu55}; *yap*^{fu48}*wwtr*$^{fu55/+}$) embryos for *yap* and *taz* were used for assessing the number of apoptotic (E,G) and proliferating cells (F,H) within the hindbrain boundaries (E-F; Table 2) or r5 (G-H; Table 3). Note that upon dowregulation of Yap in *taz* mutants, and when at least three of the *yap/taz* alleles are mutated, the number of dividing cells specifically diminishes within the boundaries. P values for (F) are the following: *yap*$^{+/+}$*wwtr*$^{+/+}$ vs. *yap*$^{fu48/+}$*wwtr*^{fu55}, p = 0.0006; *yap*$^{+/+}$*wwtr*$^{+/+}$ vs. *yap*^{fu48}*wwtr*$^{fu55/+}$, p = 0.0042; *yap*$^{fu48/+}$*wwtr*$^{fu55/+}$ vs. *yap*$^{fu48/+}$*wwtr*^{fu55}, p < 0.0001; *yap*$^{fu48/+}$*wwtr*$^{fu55/+}$ vs. *yap*$^{fu48/+}$*wwtr*^{fu55}, p = 0.0006. Tables 2-3 provide numbers of embryos used for each genotype analysis. I-J) Tg[4xGTIIC:Gal4FF;UAS:KAEDE] embryos were injected with: UAS:DsRed as control, or with DsRed:UAS.YapDN and DsRed:UAS:TeadDN forms to genetically generate clones expressing these constructs only in the Yap/Taz-active cells. Embryos displaying clones were analyzed and the number of cells displaying DsRed in each clone was scored (I), and the position of these clones within the progenitor/differentiation domain was assessed (J). P values for (I) are the following: UAS:DsRed vs. DsRed:UAS:YapDN, p = 0.0021; UAS:DsRed vs. DsRed:UAS:TeadDN, p < 0.0001. *p≤0.05, **p≤0.01, ***p≤0.001, ****p≤0.0001. The non-parametric Mann-Whitney test was used.

TABLE 1: Cohort of embryos and datasets (Figure 4).

Datasets used in this study with corresponding information about transgenic embryos and cDNA injections. Temporal frequency of image acquisition (timestep imaging) and corresponding imaging sequences are depicted.

ID dataset	Transgenic embryo	DNA injection	Timestep imaging	Imaging sequences
170117	Tg[4xGTIIC:d2GFP]	hsp:H2B-RFP	6 min	36-49 hpf
170118	Tg[4xGTIIC:d2GFP]	hsp:H2B-RFP	6 min	40-53 hpf
170119	Tg[4xGTIIC:d2GFP]	hsp:H2B-RFP	6 min	48-65,5 hpf
170125	Tg[4xGTIIC:d2GFP]	H2B-mCherry	6 min	40-55.5 hpf
170127	Tg[4xGTIIC:d2GFP]	H2B-mCherry	7 min	42-59.5 hpf
170128	Tg[4xGTIIC:d2GFP]	H2B-mCherry	7 min	70-85 hpf
170206	Tg[4xGTIIC:d2GFP]	H2B-mCherry	7 min	40-54 hpf
170207	Tg[4xGTIIC:d2GFP]	H2B-mCherry	7 min	55-69 hpf
170208	Tg[4xGTIIC:d2GFP]	H2B-mCherry	7 min	70-86.2 hpf
170215	Tg[4xGTIIC:d2GFP]	hsp:H2B-RFP	7 min	26-41 hpf
170216	Tg[4xGTIIC:d2GFP]	hsp:H2B-RFP	7 min	26-41 hpf
170222	Tg[4xGTIIC:d2GFP]	hsp:H2B-RFP	7 min	26-41 hpf
170223	Tg[4xGTIIC:d2GFP]	hsp:H2B-RFP	7 min	26-41.4 hpf
170301a	Tg[4xGTIIC:d2GFP]	hsp:H2B-RFP	7 min	26-47 hpf
170301b	Tg[4xGTIIC:d2GFP]	hsp:H2B-RFP	7 min	26-47.2 hpf
171108	Tg[4xGTIIC:d2GFP]	hsp:H2B-RFP	7 min	26-41 hpf
171109	Tg[4xGTIIC:d2GFP]	hsp:H2B-RFP	7 min	26-41 hpf

TABLE 2: Embryos used for functional analysis in the hindbrain boundaries (Figure 5)

Numbers indicate embryos used for the analysis and the number of boundaries analyzed for Figure 5.

FIGURE	GENOTYPE	# boundaries	# embryos
Figure 5A	MO-Control *wwtr*$^{+/+}$	28	7
	MO-Control *wwtr*$^{fu55/+}$	108	27
	MO-Control *wwtr*^{fu55}	52	13
	MO-Yap *wwtr*$^{+/+}$	36	9
	MO-Yap *wwtr*$^{fu55/+}$	88	22
Figure 5B	MO-Control *wwtr*$^{+/+}$	11	7
	MO-Control *wwtr*$^{fu55/+}$	25	13
	MO-Control *wwtr*^{fu55}	19	10
	MO-Yap *wwtr*$^{+/+}$	37	19
	MO-Yap *wwtr*$^{fu55/+}$	73	37
Figure 5E	*yap*$^{+/+}$ *wwtr*$^{+/+}$	12	3
	yap$^{fu48/+}$ *wwtr*$^{fu55/+}$	28	7
	yap$^{fu48/+}$ *wwtr*^{fu55}	12	3
	yap^{fu48} *wwtr*$^{fu55/+}$	12	3
Figure 5F	*yap*$^{+/+}$ *wwtr*$^{+/+}$	22	15
	yap$^{fu48/+}$ *wwtr*$^{fu55/+}$	45	36
	yap$^{fu48/+}$ *wwtr*^{fu55}	23	15
	yap^{fu48} *wwtr*$^{fu55/+}$	22	17

TABLE 3: Embryos used for functional analysis in the rhombomers (Figure 5)

Numbers indicate embryos used for the analysis and the number of rhombomeres 5 analyzed for Figure 5.

FIGURE	GENOTYPE	# r5	# embryos
Figure 5C	MO-Control *wwtr*$^{+/+}$	7	7
	MO-Control *wwtr*$^{fu55/+}$	27	27
	MO-Control *wwtr*^{fu55}	13	13
	MO-Yap *wwtr*$^{+/+}$	9	9
	MO-Yap *wwtr*$^{fu55/+}$	22	22
Figure 5D	MO-Control *wwtr*$^{+/+}$	6	6
	MO-Control *wwtr*$^{fu55/+}$	14	14
	MO-Control *wwtr*^{fu55}	10	10
	MO-Yap *wwtr*$^{+/+}$	10	10
	MO-Yap *wwtr*$^{fu55/+}$	11	11
Figure 5G	*yap*$^{+/+}$ *wwtr*$^{+/+}$	3	3
	yap$^{fu48/+}$ *wwtr*$^{fu55/+}$	7	7
	yap$^{fu48/+}$ *wwtr*^{fu55}	3	3
	yap^{fu48} *wwtr*$^{fu55/+}$	3	3
Figure 5H	*yap*$^{+/+}$ *wwtr*$^{+/+}$	13	13
	yap$^{fu48/+}$ *wwtr*$^{fu55/+}$	23	23
	yap$^{fu48/+}$ *wwtr*^{fu55}	13	13
	yap^{fu48} *wwtr*$^{fu55/+}$	12	12

SUPPLEMENTARY INFORMATION

Figure S1: Genomic edition of *yap* and *wwtr1* genes by TALEN technology

A) Scheme depicting the structure of MO-Yap and the position of the splice-blocking morpholino (MO-Yap1SB2e2i) with the corresponding primers to assess its efficiency (see green and red arrows). MO-Wwtr1 is a translation-blocking morpholino. B) Agarose gel showing the aberrant splicing products induced by morpholinos as detected by RT-PCR from embryos injected with MO-control and MO-Yap1. C-D) Embryos injected either with MO-control or MO-Yap1 and *in situ* hybridized for *myl7.* Note that upon downregulation of Yap1 embryos display defects in the migration of heart progenitors (compare C-C' with D-D') as previously described. E) Alignment of the *yap1* (yap^{fu48}) and *wwtr1* ($wwtr1^{fu55}$) mutant alleles with the corresponding wild-type sequences ($yap^{+/+}$ and $wwtr1^{+/+}$) showing the deleted nucleotides, and the TALEN target sites in the *yap1* and *wwtr1* loci with the left and right arms in magenta separated by the spacer including the restriction site used for screening (orange). F-G) Agarose gels showing the obtained bands after restriction of gDNA corresponding to embryos carrying the wild type or the mutated alleles with the corresponding enzymes. Numbers in red indicate the size of the different obtained fragments.

Figure S2: Cohort of embryos and datasets used for the cell lineage studies (Figure 4)

Plot displaying the temporal window covering the corresponding dataset.

Movie S1: Tracking of a single Yap/Taz-active boundary cell

A) Scheme depicting the outline of the experiment. Tg[4xGTIIC:d2GFP] embryos were injected at one-cell stage with hsp:H2B-RPF and heat-shocked at 26hpf. Embryos displaying red nuclei within the Yap/Taz-active boundary cells (B-B') were imaged until the desired stage (C-C'). The movie shows how a single red and green cell divides during this time window, and finally gives rise to 4 daughter cells. All cell lineages depicted in Figure 4A were obtained by tracking single cells as shown in this movie.

FIGURE 1

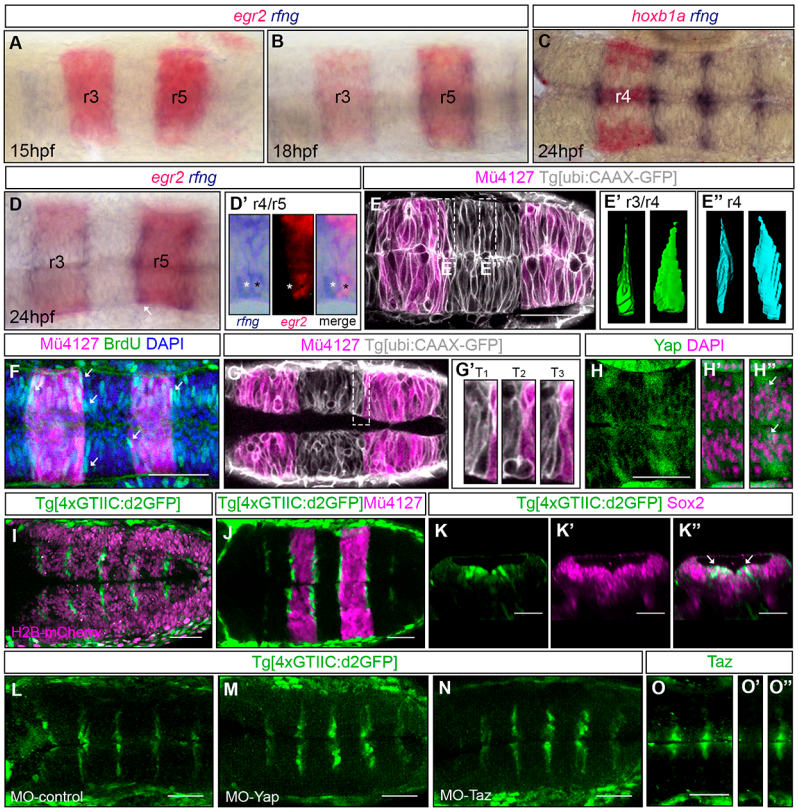
egr2 rfng
hoxb1a rfng
A
r3
r5
15hpf
B
r3
r5
18hpf
C
r4
24hpf
egr2 rfng
Mü4127 Tg[ubi:CAAX-GFP]
D
r3
r5
24hpf
D' r4/r5
rfng
egr2
merge
E
E'
E'
E' r3/r4
E" r4
Mü4127 BrdU DAPI
Mü4127 Tg[ubi:CAAX-GFP]
Yap DAPI
F
G
G' T1
T2
T3
H
H'
H"
Tg[4xGTIIC:d2GFP]
Tg[4xGTIIC:d2GFP]Mü4127
Tg[4xGTIIC:d2GFP] Sox2
I
H2B-mCherry
J
K
K'
K"
Tg[4xGTIIC:d2GFP]
Taz
L
MO-control
M
MO-Yap
N
MO-Taz
O
O'
O"

FIGURE 2

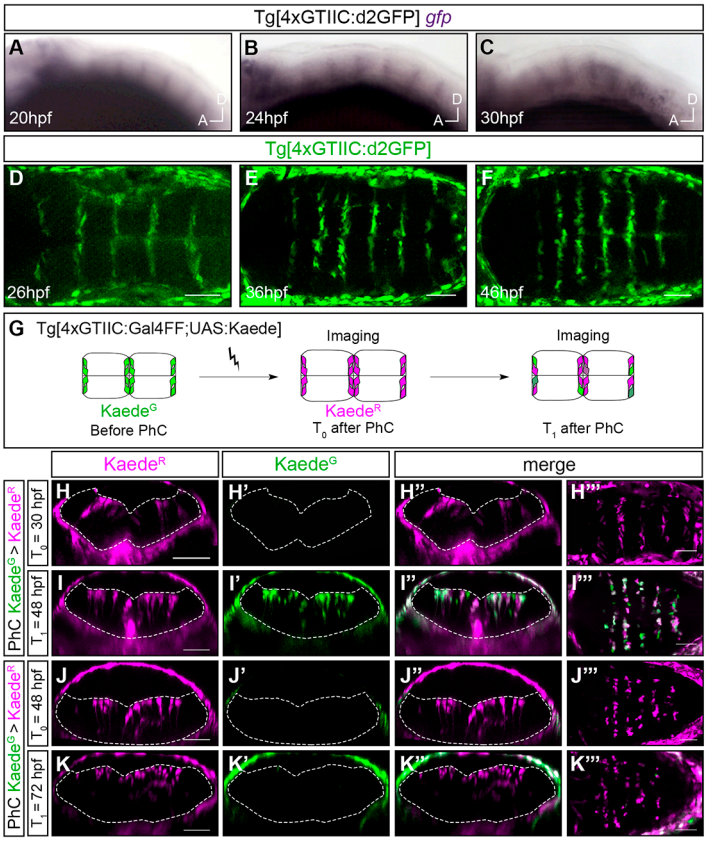
Tg[4xGTIIC:d2GFP] gfp
A
20hpf
B
24hpf
C
30hpf
Tg[4xGTIIC:d2GFP]
D
26hpf
E
36hpf
F
46hpf
G Tg[4xGTIIC:Gal4FF;UAS:Kaede]
Imaging
Imaging
KaedeG
Before PhC
KaedeR
T0 after PhC
T1 after PhC
KaedeR
KaedeG
merge
PhC KaedeG > KaedeR
T0 = 30 hpf
T1 = 48 hpf
PhC KaedeG > KaedeR
T0 = 48 hpf
T1 = 72 hpf
H
H'
H''
H'''
I
I'
I''
I'''
J
J'
J''
J'''
K
K'
K''
K'''

FIGURE 3

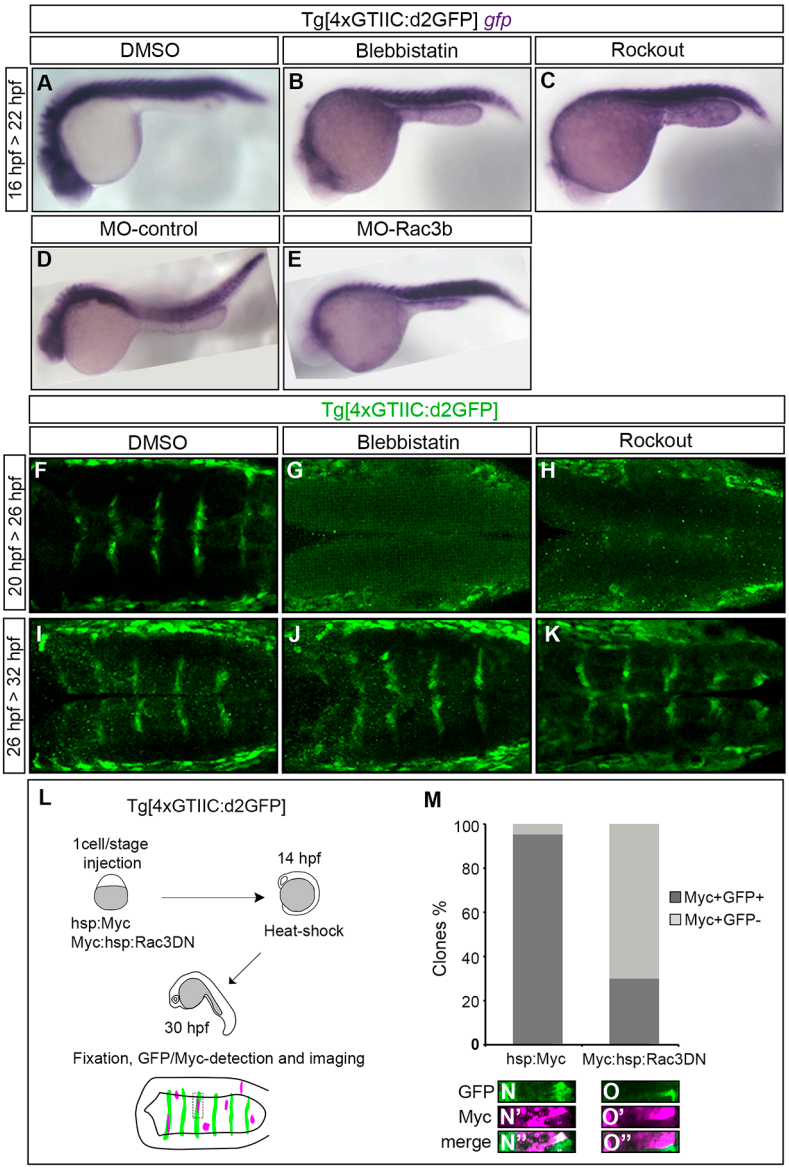
Tg[4xGTIIC:d2GFP] gfp
DMSO
Blebbistatin
Rockout
16 hpf > 22 hpf
A
B
C
MO-control
MO-Rac3b
D
E
Tg[4xGTIIC:d2GFP]
DMSO
Blebbistatin
Rockout
20 hpf > 26 hpf
F
G
H
26 hpf > 32 hpf
I
J
K
L
Tg[4xGTIIC:d2GFP]
1cell/stage injection
hsp:Myc
Myc:hsp:Rac3DN
14 hpf
Heat-shock
30 hpf
Fixation, GFP/Myc-detection and imaging
M
Clones %
100
80
60
40
20
0
Myc+GFP+
Myc+GFP-
hsp:Myc
Myc:hsp:Rac3DN
GFP
Myc
merge
N
N'
N''
O
O'
O''

FIGURE 4

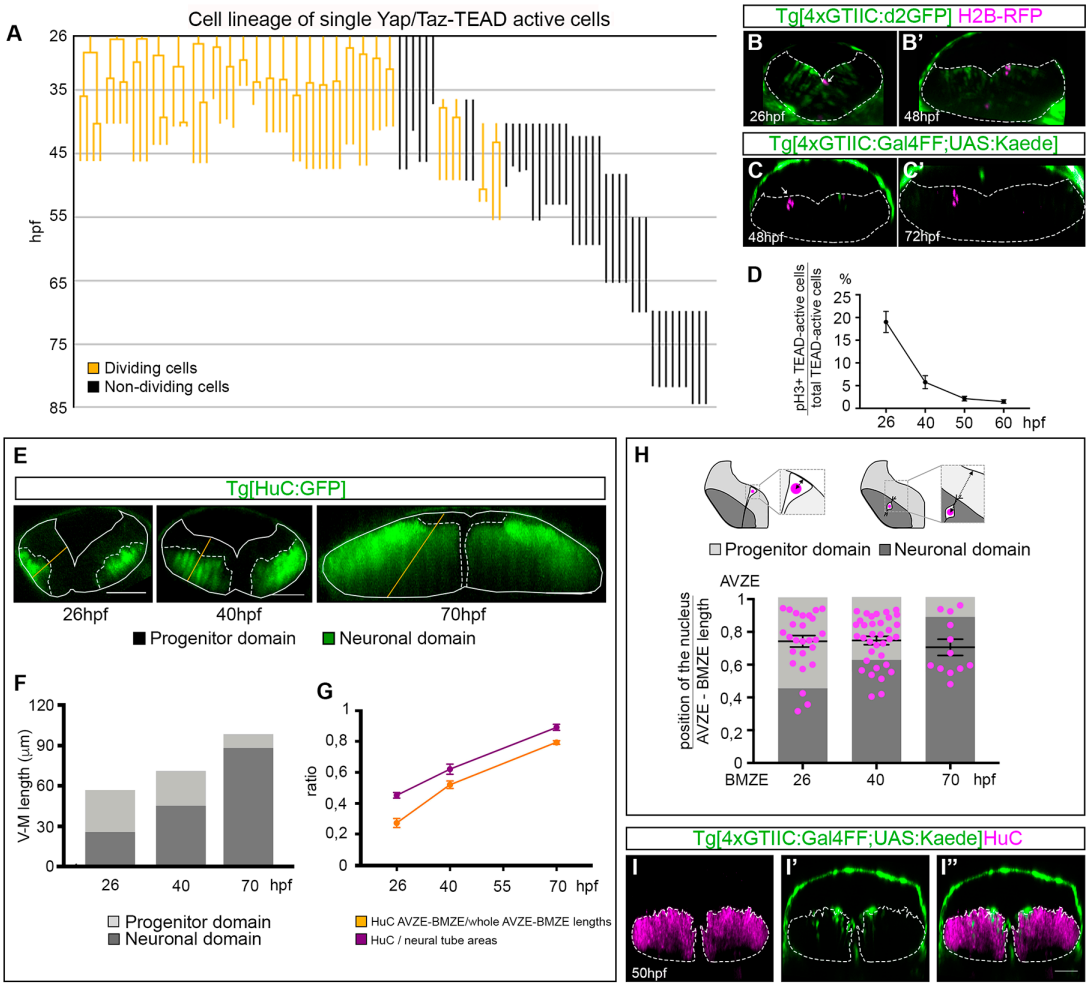
A
Cell lineage of single Yap/Taz-TEAD active cells
hpf
26
35
45
55
65
75
85
Dividing cells
Non-dividing cells
Tg[4xGTIIC:d2GFP] H2B-RFP
B
B'
26hpf
48hpf
Tg[4xGTIIC:Gal4FF;UAS:Kaede]
C
C'
48hpf
72hpf
D
pH3+ TEAD-active cells / total TEAD-active cells
%
25
20
15
10
5
0
26
40
50
60
hpf
E
Tg[HuC:GFP]
26hpf
40hpf
70hpf
Progenitor domain
Neuronal domain
F
V-M length (µm)
120
90
60
30
0
26
40
70
hpf
Progenitor domain
Neuronal domain
G
ratio
1
0,8
0,6
0,4
0,2
0
26
40
55
70
hpf
HuC AVZE-BMZE/whole AVZE-BMZE lengths
HuC / neural tube areas
H
Progenitor domain
Neuronal domain
AVZE
position of the nucleus
AVZE - BMZE length
1
0,8
0,6
0,4
0,2
0
BMZE
26
40
70
hpf
Tg[4xGTIIC:Gal4FF;UAS:Kaede]HuC
I
I'
I''
50hpf

FIGURE 5

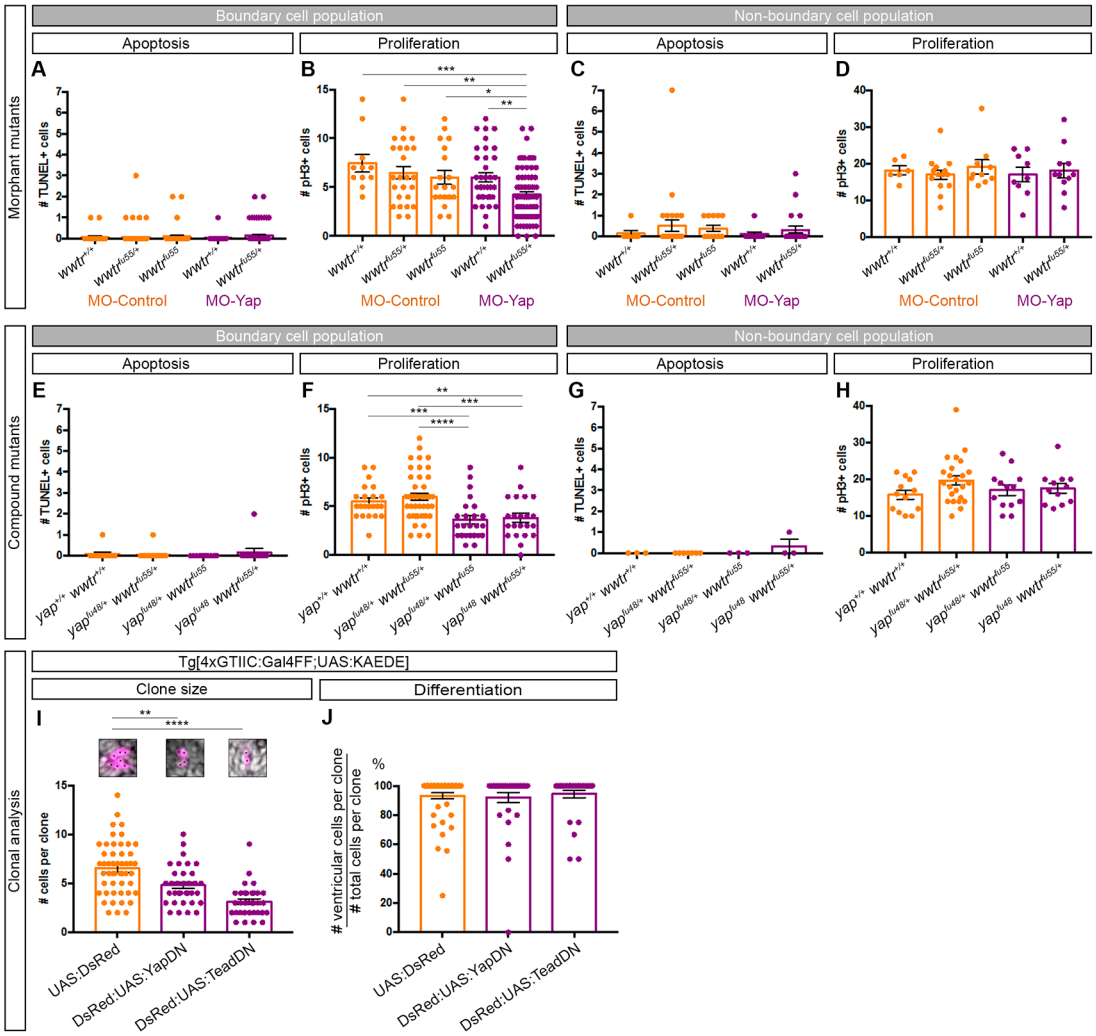
Morphant mutants
Boundary cell population
Non-boundary cell population
Apoptosis
Proliferation
A
B
C
D
TUNEL+ cells
pH3+ cells
MO-Control
MO-Yap
Compound mutants
E
F
G
H
Clonal analysis
Tg[4xGTIIC:Gal4FF;UAS:KAEDE]
Clone size
Differentiation
I
J
cells per clone
ventricular cells per clone / # total cells per clone
%
UAS:DsRed
DsRed:UAS:YapDN
DsRed:UAS:TeadDN

FIGURE S1

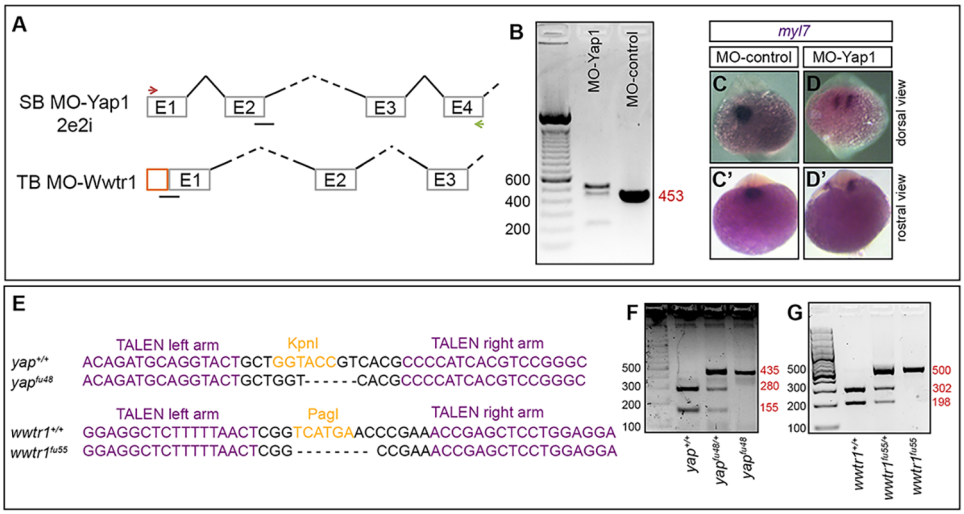
A
SB MO-Yap1
2e2i
E1
E2
E3
E4
TB MO-Wwtr1
E1
E2
E3
B
MO-Yap1
MO-control
600
400
200
453
myl7
MO-control
MO-Yap1
C
D
C'
D'
dorsal view
rostral view
E
TALEN left arm
KpnI
TALEN right arm
yap+/+ ACAGATGCAGGTACTGCTGGTACCGTCACGCCCCATCACGTCCGGGC
yapfu48 ACAGATGCAGGTACTGCTGGT------CACGCCCCATCACGTCCGGGC
TALEN left arm
PagI
TALEN right arm
wwtr1+/+ GGAGGCTCTTTTTAACTCGGTCATGAACCCGAAACCGAGCTCCTGGAGGA
wwtr1fu55 GGAGGCTCTTTTTAACTCGG-------- CCGAAACCGAGCTCCTGGAGGA
F
500
300
200
100
435
280
155
yap+/+
yapfu48+
yapfu48
G
500
300
200
100
500
302
198
wwtr1+/+
wwtr1fu55+
wwtr1fu55

FIGURE S2

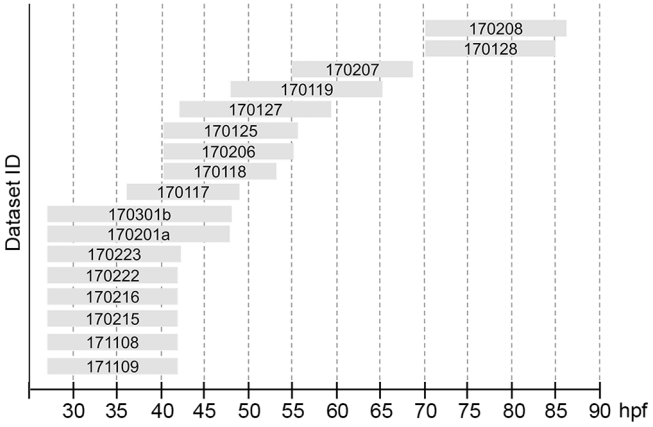
Dataset ID
170208
170128
170207
170119
170127
170125
170206
170118
170117
170301b
170201a
170223
170222
170216
170215
171108
171109
30 35 40 45 50 55 60 65 70 75 80 85 90 hpf